2024 IEEE International Conference on Robotics and Automation (ICRA 2024)
May 13-17, 2024. Yokohama, Japan

# Experimental comparison of pinwheel and non-pinwheel designs of 3D-printed cycloidal gearing for robotics

Wesley Roozing[1] and Glenn Roozing[2]

***Abstract*— Recent trends in robotic actuation have highlighted the need for low cost, high performance, and efficient gearing. We present an experimental study comparing pinwheel and non-pinwheel designs of cycloidal gearing. The open source designs are 3D-printable, combined with off-the-shelf components, achieving a high performance-to-cost ratio. Extensive experimental data is presented, that compares two prototypes on run-in behaviour and a number of quantitative metrics including transmission error, play, friction, and stiffness. Furthermore, we assess overall actuator performance through position control experiments, and a 10-hour endurance test. The results show strong performance characteristics, and crucially, suggest that non-pinwheel designs of cycloidal gearing can be a lower complexity and cost alternative to classical pinwheel designs, while offering similar performance.**

## I. Introduction

The demand for robots outside of traditional industrial environments has created new requirements and trends in robotic actuation. Traditional solutions that mostly rely on high-ratio precision strain-wave gearing do not address the new requirements sufficiently. This has generated a trend towards lower gear ratios; quasi-direct drive actuators [1]–[8]. These have shown increased efficiency, backdrivability, physical robustness, and peak speed, as well as reduced reflected inertia – making them more suitable for applications in unstructured environments, where impacts are expected.

This trend has brought into focus the need for high-performance and efficient gearing, with multiple studies being published comparing possible approaches [9]–[12]. Commonly, quasi-direct drive actuators utilise planetary, wolfrom, cycloidal, screw, and other types of transmissions, with (compound) planetary gears [13] and the related wolfrom [14], [15] being the most common. Cycloidal gears have received less attention, but offer some important benefits compared to these other options, including high torque capacity, torsional stiffness, and physical (impact) robustness [16]–[23], and several lightweight and compact cycloidal drives for robotics have been developed recently [23]–[28].

Another important requirement for robotic actuation continues to be cost. For articulated systems with many joints, actuation typically makes up the majority of the bill-of-materials, hindering adoption of robotic solutions. Many authors have recognised this and some recent works have considered low-cost design of actuation systems [4]–[8].

In our recent work [28] we proposed compact low-reduction cycloidal gearing. By leveraging 3D printing and off-the-shelf components, we developed a very high performance-to-cost design, with $\geq$40 Nm torque and the gearbox costing only €98. The developed prototype was combined with a low-cost motor and demonstrated very good performance characteristics. In this work we continue this direction, by investigating a so-called *non-pinwheel* design of cycloidal gearing, which offers significantly reduced complexity and cost. Such designs have been suggested to be able to achieve similar performance characteristics to the classical *pinwheel* design, even with free rollers [24], [29]–[32].

**Fig. 1:** Cycloidal drive prototypes: Pinwheel (left) and non-pinwheel (right) designs, with lower housing parts removed.

The contributions of this paper are as follows:

- Open source designs and design tools [33] of pinwheel and non-pinwheel cycloidal gearboxes that can be 3D printed and show high performance-to-cost ratio;
- An extensive experimental study that compares pinwheel and non-pinwheel prototypes on run-in behaviour, quantitative metrics, overall position control performance and efficiency, and an endurance test.

The remainder of this paper is outlined as follows. Sec. II describes the main geometry of pinwheel and non-pinwheel designs of cycloidal drives. Sec. III presents design considerations and the two prototypes. Sec. IV presents the extensive experimental results. Finally, Sec. V–VI conclude the paper.

## II. Working principle and main geometry

The basic geometry of a cycloidal transmission is shown in Fig. 2. Focusing first on the conventional pinwheel design (left in Fig. 2), the cycloidal disk (shown in blue), rolls over $N_\mathrm{r}$ (here 12) rollers (in black), which are located on the base circle with radius $R$. The rollers have radius $R_\mathrm{r}$, and together are referred to as the *pinwheel*. The cycloid disk is moved by an eccentric cam (shown in green) on the input shaft, with eccentricity $E$ and radius $R_\mathrm{e}$. To transfer the motion of the cycloid disk to a pure rotation of the output shaft, there are $N_\mathrm{o}$ (here 6) output holes and corresponding pins. The holes

[1]W. Roozing is with the Robotics & Mechatronics (RaM) group, University of Twente, The Netherlands. E-mail: w.roozing at utwente.nl.

[2]G. Roozing is with Auto Elect B.V., The Netherlands. E-mail: glenn.roozing at auto-elect.nl.

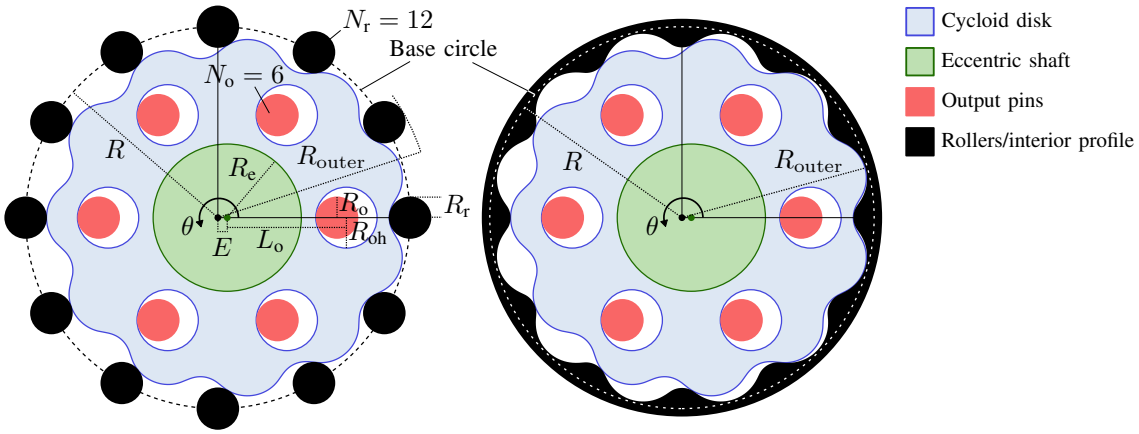


**Fig. 2:** Cycloidal drive geometry: Pinwheel (left) and non-pinwheel (right) designs.

are located at a radius $L_o$ on the disk, with radius $R_{oh}$. The output pins (shown in red) have a radius $R_o$.

The reduction ratio $n$ of a cycloidal reducer is given by

$$n = \frac{N_l}{N_r - N_l}, \tag{1}$$

where $N_l$ denotes the number of lobes on the cycloidal disk. However, it was shown that a tooth difference of one, $N_r - N_l = 1$, maximises contact area for power transmission [34]. Therefore, we restrict ourselves to such designs, and (1) reduces to $n = N_r - 1$.

### A. Pinwheel and non-pinwheel designs

In the classical pinwheel design (left in Fig. 2), the cycloidal disk interacts with circular rollers on the base circle. These rollers may be implemented in different ways:

- Bearing-supported rollers, e.g. with ball or needle bearings [18], [20], [23];
- Sliding rollers, either sleeves on fixed pins or sliding in the housing itself [16], [29];
- Fixed or fused rollers, integrated into the housing part.

Each of these represent different levels of complexity and space requirements; for example, bearing-supported rollers are only practical in lower transmission ratio designs with fewer rollers. However, bearing-supported designs have been shown to be the most efficient, and fused rollers the least efficient [16], [18], [23]. Indeed, we utilised a bearing-supported design in our previous work [28]. It should be noted that although some models suggest constant efficiency independent of transmitted torque, experimental results show otherwise [19], [21]. However, efficiency is typically very high, especially for lower gear ratio designs [18].

An alternative approach to the design of the outer rolling elements is presented by so-called *non-pinwheel* designs [24], [29], [31], [35]. In these designs, the rollers are replaced by an internal cycloidal profile, optimised for the profile of the cycloidal disk it interacts with. In [29], Hsieh et al. effectively showed that such an optimised profile can be more efficient than a conventional pinwheel design, even with free (sliding) rollers. Furthermore, they demonstrated that the non-pinwheel design reduces vibration, stress values, and stress fluctuation. In addition, the two cycloidal profiles were also shown to be in double contact during part of meshing [30], which can improve stiffness and torque capacity.

An example of a non-pinwheel design is shown right in Fig. 2, where design parameters have been kept identical to the pinwheel design on the left. Notice that the minimum outer radius of this design is given by $R_{outer} = R - R_r + E$ (which in this example $\approx R$), whereas for a pinwheel design with free (sliding or bearing-supported) rollers, the minimum outer radius is given by $R_{outer} = R + R_r$ (see Fig. 2). Hence, with equal design parameters, the non-pinwheel design can be kept smaller. There are also practical benefits; a large number of pins, bearings, washers and other components may be removed in favour of a single housing part, simplifying construction and lowering cost.

### B. External and internal cycloidal profiles

For both the pinwheel and non-pinwheel designs shown in Fig. 2, the cycloidal disk profile may be neatly expressed by the following equations [34]:

$$\begin{aligned} c_x(\theta) &= R\cos(\theta) - R_r\cos(\theta + \psi) - E\cos(N_r\,\theta), \\ c_y(\theta) &= -R\sin(\theta) + R_r\sin(\theta + \psi) + E\sin(N_r\,\theta), \end{aligned} \tag{2}$$

where $\psi$ denotes the angle between cycloid lobe and roller:

$$\psi = \tan^{-1}\left[\frac{\sin((N_r - 1)\,\theta)}{\cos((N_r - 1)\,\theta) - \frac{R}{E\,N_r}}\right], \tag{3}$$

and $\theta \in [0, 2\pi]$ denotes the angle around the input shaft.

The internal cycloidal profile of the non-pinwheel design can be generated using the so-called *double-enveloping* method first proposed by Hwang and Hsieh [31]. This is a two-stage approach. First, the cycloidal disk is generated by enveloping one roller pin around the cycloidal disk (with a result identical to (2)). Then, the profile of the internal cycloidal profile that replaces the pinwheel is obtained by the envelope of the generated cycloidal disk as it completes a full rotation. Note that this method uses the pinwheel as a starting point for the profiles: indeed, other cycloid profiles may be generated. For example, the recent work [35] explores different tooth shapes obtained directly from an epitrochoid.

In this work we adopt the method described in [29], [31], and we refer the reader to those papers for details.

## III. Pinwheel and non-pinwheel prototypes

### A. Requirements

The functional requirements of the two cycloidal drives to be designed were set to be able to reach torque and speed of medium-strength mammalian joints, at $\geq$30 Nm torque ($\sim$3 kg at 1 m) and $\geq$25 rad/s peak speed (at 48 V), respectively. We maintain the reduction ratio of $n = 11$ from our previous work [28], as well as the maximum gearbox weight of 400 g. The main drawbacks of the previous design were as follows, and will be addressed in the new designs:

- Limited torsional stiffness, leading to oscillations when driving high inertia loads and position inaccuracy;
- Use of PLA plastic, which despite high stiffness and "printability" has relatively low strength, wear resistance, and temperature resistance;
- Inability to consistently reach speeds of $>$20 rad/s due to encoder limitations, leading to current control instability.

In addition to addressing these drawbacks, we emphasise the need for cost-effective robotics components, and therefore we continue to use 3D printing with off-the-shelf steel components, while maintaining good performance characteristics. In this aspect, the non-pinwheel design has the potential to further reduce complexity and cost of cycloidal gearing.

### B. Design considerations and parameters

As described previously, the overall requirements and design approach are consistent with our previous pinwheel design [28]. Hence, the pinwheel design in this work is a refined version of the previous design, to address the drawbacks described in Sec. III-A, and the emphasis is on experimental comparison with a non-pinwheel design that is newly developed in this paper. Table I lists the design parameters for both. Note that compared to [28], the output hole location $L_\mathrm{o}$ was increased from 24.90 to 26.05 mm, to reduce linear forces on the output pins. We refer to [28] for helpful guidelines to select these parameters.

**TABLE I:** Geometric design parameters for both designs.

| | | |
|---|---|---|
| $R$ | 41.5 mm | Base circle radius (location of rollers) |
| $N_\mathrm{r}$ | 12 | Number of rollers |
| $N_\mathrm{o}$ | 6 | Number of output pins |
| $R_\mathrm{r}$ | 4.5 mm | Roller radius (bearing) |
| $R_\mathrm{o}$ | 4.5 mm | Output pin radius (bearing) |
| $E$ | 2.025 mm | Eccentricity |
| $L_\mathrm{o}$ | 26.05 mm | Output hole midpoint location |
| $R_\mathrm{oh}$ | 6.525 mm | Output hole radius |
| $R_\mathrm{e}$ | 16 mm | Eccentric shaft radius |

Different materials and production methods were considered for the new designs. Nylon (PA6) is a widely used engineering plastic for moving parts, including bushings, gears, rollers, and so on, due to its excellent strength, self-lubrication, low friction, and wear resistance properties. Reinforcement with carbon or glass fibres is often used to improve certain properties; stiffness in particular. We selected PA6-CF (Fibertree F3 PA-CF Pro, 15% carbon fibre). Finally, improvements due to more accurate manufacturing methods were considered; a selective laser sintering (SLS) prototype was briefly investigated but showed no additional benefit over a fused deposition modelled (FDM) prototype fabricated with a well-calibrated consumer-grade Prusa i3 MK3S+.

### C. CAD and prototypes

Section and 3D CAD diagrams of the pinwheel and non-pinwheel design are shown in Fig. 3, indicating the eccentric shaft (A), output disk (B), cycloid disks (C), roller pins (D), output pins (E), stiffness ring (F), and non-pinwheel internal cycloidal profile (G). Shoulder screws are used to accurately position bearings, where applicable (output pins, and rollers for the pinwheel design). All bearings, screws, etc. are off-the-shelf components, leading to a bill-of-materials cost of €98 and €65 (-33%) for the pinwheel and non-pinwheel designs, respectively. For fair comparison, the non-pinwheel was not optimised but designed as an otherwise identical drop-in replacement. Both gearboxes are combined with a T-Motor Antigravity 8012 brushless motor, 14-bit CUI AMT23 motor encoder, and optional 14-bit AMS AS5048A output encoder. We refer to Table II for full specifications, including comparison to our previous design [28]. Finally, the realised prototypes are shown in Fig. 1. These designs are open source, with CAD STL/STEP and design tools provided [33].

**TABLE II:** Prototype specifications.

| | **Prev.** [28] | **Pinwheel** | **Non-pin** | |
|---|---|---|---|---|
| Reduction ratio $n$ | 11 | 11 | 11 | - |
| Nominal torque (40 A) | 36.4 | 36.4 | 36.4 | Nm |
| Peak speed | 20 | 28 | 28 | rad/s |
| Gearbox mass | 372 | 377 | 360 | g |
| Gearbox thickness | 23 | 23 | 23 | mm |
| Gearbox diameter | 104 | 104 | 104 | mm |
| Bill-of-materials cost | 98 | 98 | **65** | € |

## IV. Experimental results

The prototypes are validated through a series of experiments. We compare run-in behaviour of the two prototypes, and gearing performance quantitatively in terms of transmission error, play, friction, and stiffness. Furthermore, we assess overall actuator performance through position control experiments with different loads, and an endurance test.

The experimental setup comprises table fixture and output flange with optional (vertical) pendulum. Experiments were conducted with a 40 V power supply and an ODrive Robotics v3.6, which received commands through its Python/serial interface. Position, velocity and reference/measured current data were logged via the serial interface.

### A. Initial run-in

Before any other experiments, we assess run-in behaviour of both prototypes. The actuators were ran at 8 rad/s output speed for 90 minutes (5400s). Fig. 4 shows motor current over this time. Apart from an initial rapid drop in current for

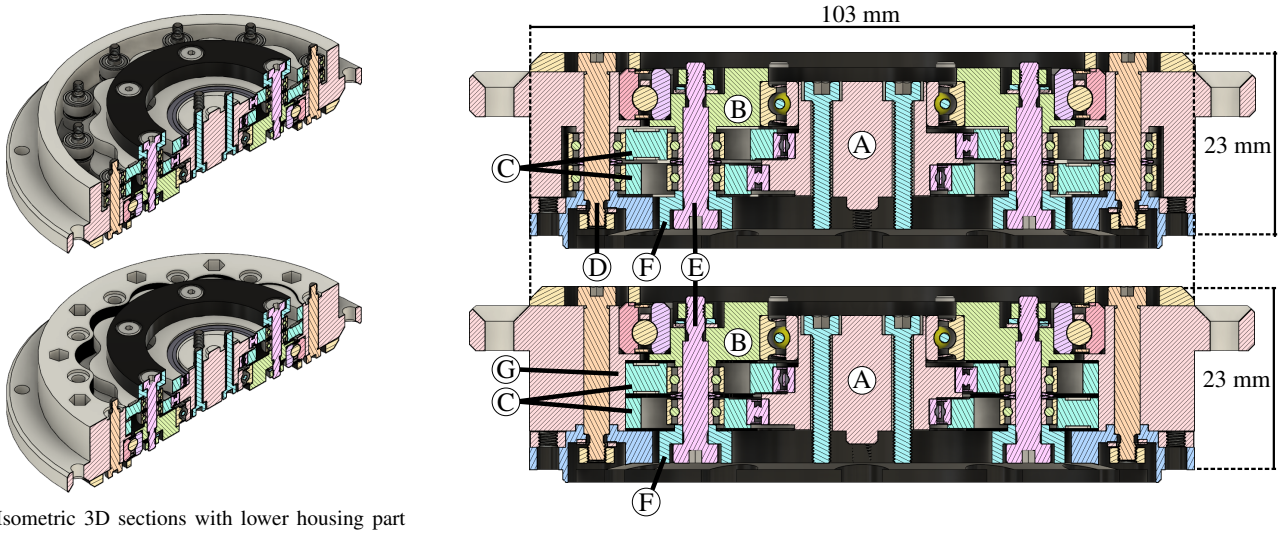


**(a)** Isometric 3D sections with lower housing part removed, showing cycloid profiles.

**(b)** Section views.

**Fig. 3:** CAD of the pinwheel (top) and non-pinwheel (bottom) designs.

the pinwheel design, both actuators demonstrate very similar run-in, with the majority of change occurring in the first 30 minutes (1800s). This demonstrates that interaction of the two cycloidal profiles of the non-pinwheel design does not negatively affect (unloaded) friction during or after run-in.

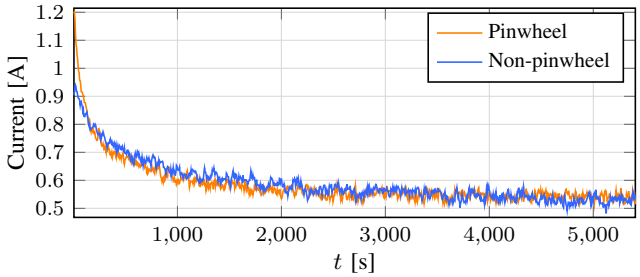


**Fig. 4:** Run-in: 90 minutes at 8 rad/s output speed.

### B. Transmission error, play, and friction

After the initial run-in, we validate basic gearing performance of both actuators, starting with transmission error. The actuators were controlled to a constant output speed of $\dot{q} = 2.0$ rad/s, and the difference between reduced input and output positions measured using the motor and output encoders. This difference is given by $\theta/n - q$. Fig. 5 shows the result for both prototypes. The pinwheel and non-pinwheel prototypes show an RMS transmission error of 0.38 deg and 0.56 deg respectively, with maxima of 0.7 deg and 1.0 deg, respectively. Despite the larger error for the non-pinwheel design, this amounts to approximately 5% maximum variation in gear ratio (i.e., velocity ripple) for both cases[1]. This is relatively good compared to other cycloidal gearing designs [16], [22], including our previous work [28].

[1]Gear ratio variation and positioning error are typically different because transmission ratio relates velocities, and positioning inaccuracy is accrued only when variation in this ratio is integrated over displacement.

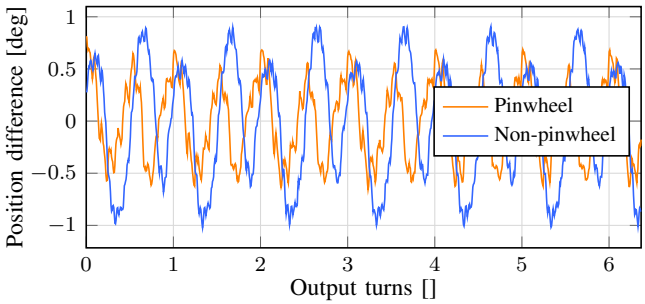


**Fig. 5:** Transmission error, measured as position difference $\theta/n - q$.

Play in the transmissions was estimated by measurements of maximum possible output displacement that would not cause movement of the motor, around different positions of the output. For both prototypes, typical play was approx. 0.20 to 0.25 deg (∼2 mm at 50 cm from the rotation point), with maxima of 0.35 and 0.30 deg for the pinwheel and non-pinwheel designs respectively.

Finally, Coulomb friction was estimated at 0.62 and 0.53 Nm, respectively, by slowly ramping output velocity between ±10 rad/s, and measuring required torque. Note that these values depend heavily on run-in (Sec. IV-A) as well as temperature, and more elaborate characterisation of friction and efficiency is part of ongoing work. The numerical results of all of these tests are summarised in Table IV, where they are also compared to our previous work [28].

### C. Gearing stiffness

We estimate the internal stiffness of both prototypes by fixing the output and applying increasing motor current. As the output is fixed ($q \equiv 0$), the internal deflection is given by $\theta/n - q = \theta/n$. Motor current is slowly ramped from 0 A to 40 A, and back down, in both positive and negative directions. Linearity of the current-torque relationship in this range was validated a priori. We fit a linear curve of the shape $\theta = \hat{k}^{-1}\,\tau_{\mathrm{m}} + b$, where the slope defines the estimated

stiffness $\hat{k}$ in Nm/rad. This is performed separately in both directions, and the result is averaged to obtain a final stiffness estimate. Although a multi-segment curve could have been used to account for stiffening effects, we do not consider that useful given the presence of significant hysteresis here.

The results are shown in Fig. 6, and the stiffness estimates are listed in Table III. Fig. 6 shows the fit results as dashed lines. Both prototypes show a stiffening behaviour, and significant hysteresis between the loading and unloading directions. Both effects are stronger for the non-pinwheel design. We believe the increased stiffening of the non-pinwheel design is due to the larger contact surface area between the two cycloidal profiles, compared to the pinwheel design where the cycloidal disk is in contact only with the circular roller bearing. The increased hysteresis may indicate deflection of the PA-CF internal cycloidal profile for that case, in addition to deflection of the identical inner components that both designs experience.

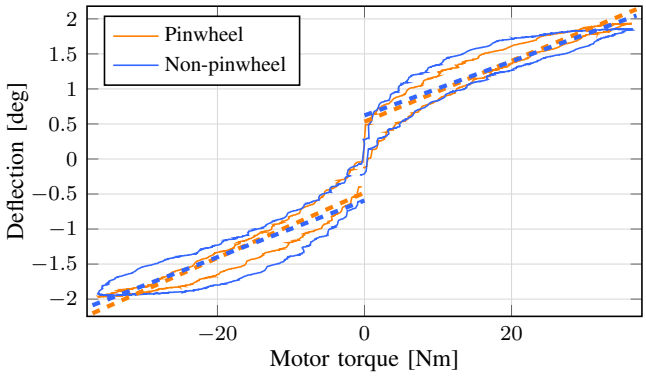


**Fig. 6:** Transmission stiffness.

**TABLE III:** Estimated stiffness values.

| | Forward | Backward | **Mean** ($\hat{k}$) |
|---|---|---|---|
| Pinwheel | 1325 | 1217 | **1271 [Nm/rad]** |
| Non-pinwheel | 1493 | 1442 | **1468 [Nm/rad]** |

### D. Position control

We validate overall drive performance by performing point-to-point motion control experiments on both prototypes, each with two loads; a 380 g, 0.025 kg m$^2$ pendulum, and a 2.66 kg, 0.5 m, 0.59 kg m$^2$ pendulum, both lifted against gravity. We generate continuous velocity profiles between the waypoints using the ODrive's trajectory control, with maximum velocity and acceleration limited to 30 rad/s, 120 rad/s$^2$, and 15 rad/s, 15 rad/s$^2$, respectively[2]. In all cases, the next waypoint was set immediately when the actuator was within 0.01 rad of the currently desired position.

The results are shown in Figs. 7 and 8. Both prototypes yield very similar results, including velocity and current profiles. This suggests no significant difference in friction or efficiency of both prototypes in these dynamic tasks. For the light pendulum in Fig. 7, the non-pinwheel prototype manages to complete the full trajectory slightly ahead of the pinwheel prototype. Both reach a peak speed just over 27 rad/s. For the heavy pendulum in Fig. 8, the results are again very similar between the two prototypes[3], and significantly better than those with the previous prototype [28], where we observed significant velocity and current oscillations due to limited stiffness of the gearbox. This confirms the increased stiffness measured in Sec. IV-C, and the effectiveness of the redesign for increased stiffness. Finally, motor current can be observed to be nearly identical between the two prototypes, demonstrating similar efficiency of the two designs also in this higher torque scenario.

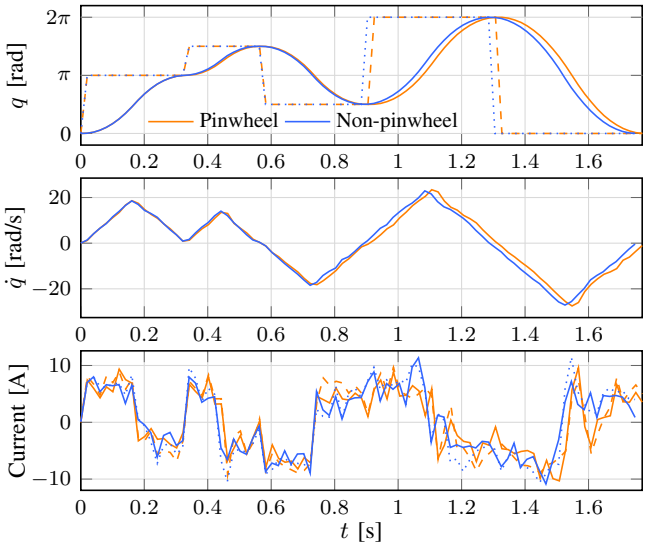


**Fig. 7:** Position control with 380 g, 0.025 kg m$^2$ pendulum: Position, velocity, and current over time (position and velocity from motor encoder). Dashed and dotted lines denote references.

### E. Endurance test

Finally, after completion of the previous experiments, both gearboxes were subjected to a 10 hour endurance test, in 1 hour intervals. The test comprised a motion profile performed with the heavy pendulum, reaching torques and speeds of over 15 Nm and 3 rad/s respectively. Over the 10 hours both prototypes completed 1390 motion cycles each. Results are shown in Fig. 9. The mean position, velocity, and current profile of each of the 10 hours is shown. Cycle-to-cycle variance was negligible and too small to show visually. Hour-to-hour differences are also very small, with curves for each actuator overlapping nearly perfectly. There are minor differences between the pinwheel and non-pinwheel designs, particularly oscillations in velocity and current for the pinwheel design, which may be due to lower stiffness.

## V. Discussion

Table IV summarises the quantitative performance results of the two cycloidal drives, and compares them to our

[2]The video attachment shows even more aggressive results, at 160 rad/s$^2$ and 20 rad/s$^2$ acceleration, respectively.

[3]There is a peak in the velocity data upon changes of acceleration direction, for both prototypes. This is a result of the small amount of play present as well as lower initial stiffness and acceleration feed-forward.

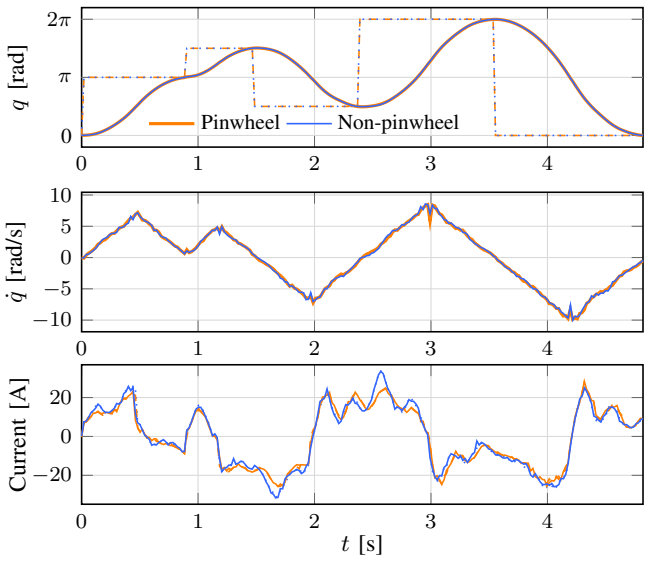


**Fig. 8:** Position control with 2.66 kg, 0.59 kg m$^2$ pendulum: Position, velocity, and current over time (position and velocity from motor encoder). Dashed and dotted lines denote references.

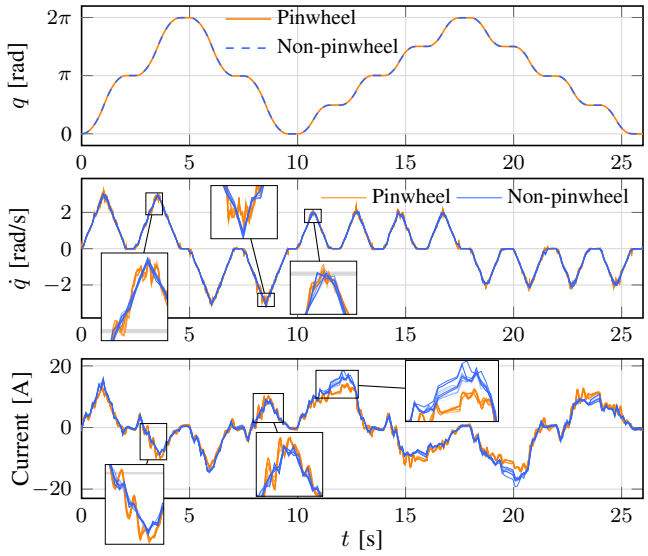


**Fig. 9:** Endurance test: 10 hours (1390 cycles of shown motion profile) of position control with 2.66 kg, 0.59 kg m$^2$ pendulum, for both prototypes. Mean position, velocity, and current for each hour is shown (10 curves overlayed with increasing opacity per hour).

previous work [28] for comparison. Overall, the two new drives significantly outperform the previous design in terms of transmission error, gear ratio variation, at the cost of slightly increased friction. Importantly, stiffness increased significantly (over 2x). Finally, using another low-cost encoder allowed the new prototypes to reach 28 rad/s peak speed. Therefore, both new prototypes successfully address the main drawbacks of the previous design.

Comparing the new pinwheel and non-pinwheel gearing designs, a slightly larger transmission error is noted for the non-pinwheel design (although this may be within manufacturing tolerance), as well as larger torsional stiffness. We believe that the increased stiffness is due to larger contact area between the cycloidal disk and interior cycloid profile of the non-pinwheel design. Otherwise, the quantitative results demonstrate high similarity between the two. Furthermore, the position control experiments in Sec. IV-D show nearly identical responses of the two new prototypes, suggesting comparable efficiency in dynamic motions.

Crucially, none of the results suggest a performance disadvantage for non-pinwheel designs, which should be otherwise preferred over pinwheel based designs because of their reduced cost and complexity. We note that the current non-pinwheel design is not optimised, that is, it was designed as a drop-in replacement for the pinwheel design. A fully optimised design will be able to reduce cost and mass, as well as either reduce size or increase the diameter of gearing parts, to improve torsional strength and stiffness.

Finally, the endurance test showed very consistent behaviour over 10 hours, for both prototypes. However, we did find a significant increase in play for both prototypes after this test (∼2x); microscope inspection revealed uneven wear on the outside of the cycloidal disks and inside the housing cycloid. It appears the cycloid disks' outer surfaces were not completely flat, showing 'elephant's foot' type deviations. Having worn away, their removal causes increased play in the mechanism. We believe these issues may be solved by adjusting printing calibration and dimensional adjustment of the disks combined with an extended run-in time.

**TABLE IV:** Performance overview of pinwheel and non-pinwheel designs. We report results of our previous work [28] for comparison.

| | Prev. [28] | **Pinwheel** | **Non-pin** | |
|---|---|---|---|---|
| Transmission err. | 0.92 | 0.38 | 0.56 | deg RMS |
| | 1.8 | 0.7 | 1.0 | deg max |
| Ratio variation | ∼9% | ∼5% | ∼5% | - |
| Play | - | 0.20-0.25 | 0.20-0.25 | deg typ. |
| | 0.35 | 0.35 | 0.30 | deg max |
| Coulomb friction | 0.41 | 0.62 | 0.53 | Nm |
| Stiffness | 633 | 1271 | 1468 | Nm/rad |
| Mass | 372 | 377 | 360 | g |

## VI. Conclusions & Future Work

This paper has presented an extensive experimental comparison of pinwheel and non-pinwheel designs of cycloidal gearing for robotics. Leveraging 3D printing with off-the-shelf steel components, we developed two open-source prototypes that show high performance-to-cost ratio. Our experimental results do not show a significant performance disadvantage for the non-pinwheel design, compared to the traditional pinwheel design. Due to their significantly reduced complexity and cost, this suggests that non-pinwheel designs based on internal cycloidal profiles may be a fruitful avenue towards developing lost-cost actuation systems for robots. Future work should further investigate the friction and efficiency of both types of designs while loaded, mapping these variables over torque and speed. Secondly, trade-offs in part design, 3D printing, and run-in appear to be crucial and should be further analysed.

## References


[1] P. M. Wensing *et al.*, "Proprioceptive actuator design in the MIT cheetah: Impact mitigation and high-bandwidth physical interaction for dynamic legged robots," *IEEE Transactions on Robotics*, 2017. DOI: 10.1109/TRO.2016.2640183.

[2] S. Yu *et al.*, "Quasi-direct drive actuation for a lightweight hip exoskeleton with high backdrivability and high bandwidth," *IEEE/ASME Transactions on Mechatronics*, vol. 25, no. 4, Aug. 2020. DOI: 10.1109/TMECH.2020.2995134.

[3] H. Zhu, C. Nesler, N. Divekar, V. Peddinti, and R. D. Gregg, "Design principles for compact, backdrivable actuation in partial-assist powered knee orthoses," *IEEE/ASME Transactions on Mechatronics*, vol. 26, no. 6, Dec. 2021. DOI: 10.1109/TMECH.2021.3053226.

[4] B. Katz, J. D. Carlo, and S. Kim, "Mini cheetah: A platform for pushing the limits of dynamic quadruped control," in *2019 International Conference on Robotics and Automation (ICRA)*, May 2019. DOI: 10.1109/ICRA.2019.8793865.

[5] N. Kau, A. Schultz, N. Ferrante, and P. Slade, "Stanford doggo: An open-source, quasi-direct-drive quadruped," in *2019 International Conference on Robotics and Automation (ICRA)*, May 2019. DOI: 10.1109/ICRA.2019.8794436.

[6] D. V. Gealy *et al.*, "Quasi-direct drive for low-cost compliant robotic manipulation," *arXiv:1904.03815 [cs]*, Apr. 2019. arXiv: 1904.03815.

[7] F. Grimminger *et al.*, "An open torque-controlled modular robot architecture for legged locomotion research," *IEEE Robotics and Automation Letters*, vol. 5, no. 2, Apr. 2020. DOI: 10.1109/LRA.2020.2976639.

[8] K. Urs, C. E. Adu, E. J. Rouse, and T. Y. Moore, "Design and characterization of 3d printed, open-source actuators for legged locomotion," in *2022 IEEE/RSJ International Conference on Intelligent Robots and Systems (IROS)*, Oct. 23, 2022. DOI: 10.1109/IROS47612.2022.9981940.

[9] N. Kashiri *et al.*, "An overview on principles for energy efficient robot locomotion," *Frontiers in Robotics and AI*, vol. 5, Dec. 11, 2018. DOI: 10.3389/frobt.2018.00129.

[10] P. L. García, S. Crispel, E. Saerens, T. Verstraten, and D. Lefeber, "Compact gearboxes for modern robotics: A review," *Frontiers in Robotics and AI*, vol. 7, Aug. 2020. DOI: 10.3389/frobt.2020.00103.

[11] B. Laschowski and J. McPhee, "Energy-efficient actuator design principles for robotic leg prostheses and exoskeletons: A review of series elasticity and backdrivability," *Journal of Computational and Nonlinear Dynamics*, vol. 18, no. 6, Jun. 1, 2023. DOI: 10.1115/1.4056919.

[12] E. Saerens *et al.*, "Scaling laws for robotic transmissions," *Mechanism and Machine Theory*, vol. 140, Oct. 2019. DOI: 10.1016/j.mechmachtheory.2019.06.027.

[13] H. Matsuki, K. Nagano, and Y. Fujimoto, "Bilateral drive gear—a highly backdrivable reduction gearbox for robotic actuators," *IEEE/ASME Transactions on Mechatronics*, vol. 24, no. 6, Dec. 2019. DOI: 10.1109/TMECH.2019.2946403.

[14] S. Crispel *et al.*, "A novel wolfrom-based gearbox for robotic actuators," *IEEE/ASME Transactions on Mechatronics*, vol. 26, no. 4, Aug. 2021. DOI: 10.1109/TMECH.2021.3079471.

[15] P. L. Garcia *et al.*, "R2power: The proof-of-concept of a backdrivable, high-ratio gearbox for human-robot collaboration," in *International Conference on Robotics and Automation (ICRA)*, May 23, 2022. DOI: 10.1109/ICRA46639.2022.9811923.

[16] J. W. Sensinger and J. H. Lipsey, "Cycloid vs. harmonic drives for use in high ratio, single stage robotic transmissions," in *2012 IEEE International Conference on Robotics and Automation*, May 2012. DOI: 10.1109/ICRA.2012.6224739.

[17] J. W. Sensinger, "Unified approach to cycloid drive profile, stress, and efficiency optimization," *Journal of Mechanical Design*, vol. 132, no. 2, Feb. 2010. DOI: 10.1115/1.4000832.

[18] J. W. Sensinger, "Efficiency of high-sensitivity gear trains, such as cycloid drives," *Journal of Mechanical Design*, vol. 135, no. 7, Jul. 2013. DOI: 10.1115/1.4024370.

[19] L. C. Farrell, J. Holley, W. Bluethmann, and M. K. O'Malley, "Cycloidal geartrain in-use efficiency study," in *Volume 5B: 42nd Mechanisms and Robotics Conference*, Aug. 2018. DOI: 10.1115/DETC2018-85275.

[20] K Olejarczyk, M Wikło, and K Kołodziejczyk, "The cycloidal gearbox efficiency for different types of bearings—sleeves vs. needle bearings," *Proceedings of the Institution of Mechanical Engineers, Part C: Journal of Mechanical Engineering Science*, vol. 233, no. 21, Nov. 2019. DOI: 10.1177/0954406219859903.

[21] K. Olejarczyk, M. Wikło, K. Kołodziejczyk, R. Król, and K. Król, "Theoretical and experimental verification of one stage cycloidal gearbox efficiency," in *Advances in Mechanism and Machine Science*, T. Uhl, Ed., vol. 73, Series Title: Mechanisms and Machine Science, Springer International Publishing, 2019. DOI: 10.1007/978-3-030-20131-9_102.

[22] M Wikło, R Król, K Olejarczyk, and K Kołodziejczyk, "Output torque ripple for a cycloidal gear train," *Proceedings of the Institution of Mechanical Engineers, Part C: Journal of Mechanical Engineering Science*, vol. 233, no. 21, Nov. 2019. DOI: 10.1177/0954406219841656.

[23] K. Lee, S. Hong, and J.-H. Oh, "Development of a lightweight and high-efficiency compact cycloidal reducer for legged robots," *International Journal of Precision Engineering and Manufacturing*, vol. 21, no. 3, 2019. DOI: 10.1007/s12541-019-00215-9.

[24] T. Lenzi, J. Lipsey, and J. W. Sensinger, "The RIC arm—a small anthropomorphic transhumeral prosthesis," *IEEE/ASME Transactions on Mechatronics*, vol. 21, no. 6, Dec. 2016. DOI: 10.1109/TMECH.2016.2596104.

[25] J. White, D. Swart, and C. Hubicki, "Force-based control of bipedal balancing on dynamic terrain with the "tallahassee cassie" robotic platform," in *IEEE International Conference on Robotics and Automation (ICRA)*, May 2020. DOI: 10.1109/ICRA40945.2020.9196725.

[26] H. Yamato *et al.*, "A partner robot transforming to a vehicle: CanguRo - design, development and evaluation of its in-wheel drive unit with cycloid gear," in *IEEE/SICE International Symposium on System Integration (SII)*, Jan. 2020. DOI: 10.1109/SII46433.2020.9025922.

[27] A. Kakogawa *et al.*, "A highly backdrivable robotic arm using low friction and high accuracy cycloidal geared motors: ALFHA," in *IEEE/SICE International Symposium on System Integration (SII)*, Jan. 9, 2022. DOI: 10.1109/SII52469.2022.9708868.

[28] W. Roozing and G. Roozing, "3d-printable low-reduction cycloidal gearing for robotics," in *2022 IEEE/RSJ International Conference on Intelligent Robots and Systems (IROS)*, Oct. 23, 2022. DOI: 10.1109/IROS47612.2022.9982006.

[29] C.-F. Hsieh, "Dynamics analysis of cycloidal speed reducers with pinwheel and nonpinwheel designs," *Journal of Me-*

*chanical Design*, vol. 136, no. 9, Sep. 1, 2014. DOI: 10.1115/1.4027850.

[30] B. Chen, H. Zhong, J. Liu, C. Li, and T. Fang, "Generation and investigation of a new cycloid drive with double contact," *Mechanism and Machine Theory*, vol. 49, Mar. 2012. DOI: 10.1016/j.mechmachtheory.2011.10.001.

[31] Y.-W. Hwang and C.-F. Hsieh, "Geometric design using hypotrochoid and nonundercutting conditions for an internal cycloidal gear," *Journal of Mechanical Design*, vol. 129, no. 4, Apr. 2007. DOI: 10.1115/1.2437806.

[32] C.-F. Hsieh and A. Fuentes-Aznar, "Performance prediction method of cycloidal speed reducers," *Journal of the Brazilian Society of Mechanical Sciences and Engineering*, vol. 41, no. 4, Apr. 2019. DOI: 10.1007/s40430-019-1690-2.

[33] W. Roozing and G. Roozing. "Cycloidal-drive-nonpinwheel." (Aug. 16, 2023), [Online]. Available: https://github.com/geez0x1/2023-cycloidal-drive-nonpinwheel.

[34] J.-H. Shin and S.-M. Kwon, "On the lobe profile design in a cycloid reducer using instant velocity center," *Mechanism and Machine Theory*, vol. 41, no. 5, May 2006. DOI: 10.1016/j.mechmachtheory.2005.08.001.

[35] D.-J. Jang, Y.-C. Kim, E.-P. Hong, and G.-S. Kim, "Geometry design and dynamic analysis of a modified cycloid reducer with epitrochoid tooth profile," *Mechanism and Machine Theory*, vol. 164, Oct. 2021. DOI: 10.1016/j.mechmachtheory.2021.104399.